4B.4 SENSITIVITY STUDY ON NUDGING PARAMETERS FOR A MESOSCALE FDDA SYSTEM

Mei Xu[1], Yubao Liu, Chris A. Davis and Thomas T. Warner

National Center for Atmospheric Research[2], Boulder, Colorado

1. INTRODUCTION

A mesoscale real-time four-dimensional data assimilation (RT-FDDA) and short-term forecasting system has been developed at NCAR/RAP for the U.S. Army Test and Evaluation Command (ATEC) at the White Sand Mission Range (WSMR). Built on the Penn State/NCAR mesoscale model (MM5), the system continuously assimilates available observations from various sources and provides updated 3-dimensional analyses and short-term forecasts every 3 hours. The data assimilation engine is based on the Newtonian Relaxation (nudging) method. Details of the system and its general performance evaluation can be found in Cram et al. (2001) and Liu et al. (2002).

Previously the nudging method was mostly tested on the synoptic scale. Few studies have been done with a fine resolution grid (grid increment of 1-3 km) that can resolve fine scale terrain and very local circulations. At the fine scale, choosing the appropriate nudging parameters, such as (1) the influence radius of observations, (2) nudging coefficients and (3) weighting functions, may have a critical effect on the data assimilation result.

A series of sensitivity simulations are conducted in this study by gradually changing the three nudging parameters in the RT-FDDA system. A clear-sky case with life-cycles of local thermally driven circulations is chosen for the tests. The methodologies and some preliminary results are described in this paper.

2. SPECIFICATION OF THE PROBLEM

The approach of the Newtonian relaxation or nudging method is to relax the model state toward the observed state by adding, to one or more of the prognostic equations, artificial tendency terms based on the difference between the two states. The model solution can be nudged toward either gridded analyses or individual observations. Observational nudging is performed in the RT-FDDA system using traditional observations (rawinsonde, metar, ship/buoy reports), as well as non-traditional observations (mesonet, aircraft reports, profilers and satellite wind).

1. Corresponding author address: Mei Xu, NCAR/RAP, P.O. Box 3000, Boulder, Colorado 80307-3000. E-mail: meixu@ucar.edu

2. The National Center for Atmospheric Research is sponsored by the National Science Foundation.

In observational nudging, the difference between the model state and the observed state is computed at the observation locations, and analyzed back to the grid in a region surrounding the observations. At a given time step and grid point (**x**,t), the tendency term that is added to the equations is proportional to

$$G_\alpha \bullet \sum_{i=1}^{N} W_i^{\,2}(x,t)\,\gamma_i(\alpha_{ob}-\alpha)_i \Big/ \sum_{i=1}^{N} W_i(x,t)$$

Where the summation is over all the observations within an influence radius of the given grid point. The observational quality factor, γ, ranges from 0 to 1.

The nudging coefficient G_α determines the relative magnitude of the nudging term. Under simplified conditions, the model state approaches the observed state exponentially with an e-folding time of $(1/G_\alpha)$. Therefore relatively large G_α should be used to effectively nudge high frequency data. On the other hand, G_α should be small such that the nudging term is small compared to the total tendency term in the prognostic equation.

The weighting for observation *i* is determined by the spatial and temporal separation of the observation and the grid point, and can be written as

$$W(x,t) = w_{xy} \cdot w_z \cdot w_t$$

In the current RT-FDDA system, the horizontal weighting function is a Cressman-type function

$$w_{xy} = \frac{R^2 - D^2}{R^2 + D^2} \qquad 0 \le D \le R$$

$$w_{xy} = 0 \qquad D > R$$

The vertical weighting function and the temporal weighting function are also distance weighted

$$w_z = 1 - \frac{|p_{ob} - p|}{R_z} \qquad |p_{ob} - p| \le R_z$$

$$w_z = 0 \qquad |p_{ob} - p| > R_z$$

$$w_t = 1 \qquad |t - t_{ob}| < \tau/2$$

$$w_t = \frac{\tau - |t - t_{ob}|}{\tau/2} \qquad \tau/2 \le |t - t_{ob}| \le \tau$$

$$w_t = 0 \qquad |t - t_{ob}| > \tau$$

where R and R_z are the horizontal and vertical radii of influence, and τ is the half period of a time window.

Values of the nudging parameters have to be selected empirically. In the current RT-FDDA at WSMR, the data quality factor γ is1 for all observations. The nudging factor is set to $6x10^{-4}$ s^{-1} for all variables (u,v,T,q) which is equivalent to a forcing time scale of approximately 30 minutes. The time window is +/-40 minutes around the observation valid time. The maximum horizontal influence radius R is constant for each grid, varying from grid to grid: 180 km on grid 1, 90 km on grid 2, and 60 km on grid 3.

In the case where there is a local circulation, a constant horizontal radius of influence without considering local terrain effects may result in serious errors in the model solution. As a simple example, Fig. 1 illustrates that when an observation is obtained at a site situated near a mountain ridge, the observation may not be representative of the flow on the opposite side of the mountain ridge. It would be wrong to propagate that piece of information using a circular radius of influence.

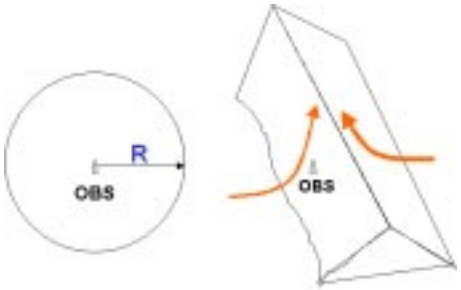

Figure 1 Schematic plot showing the need for terrain dependent nudging weights.

3. EXPERIMENTAL DESIGN

This case study is based on a clear-sky event on November 11, 2001. The current RT-FDDA system is first run for 22 h after a cold start to provide common restart files for all the sensitivity runs. Then a set of five assimilation experiments is conducted for 48 h by varying the RT-FDDA parameters and options (Table 1).

For each experimental run, sixteen analysis/forecast cycles are conducted for the 48 h period. The grid sizes are 84x98, 67x70 and 61x61 respectively for the 3 nests (Fig. 2), and the grid increments are 30 km, 10 km and 3.3 km. There are 31 vertical levels.

Table 1. Experiment list.

EXPERIMENT	DESCRIPTION
EXP1 (control)	current RT-FDDA parameters
EXP2 (no grid3 FDDA)	no observation nudging on grid 3
EXP3 (reduced R)	R =180, 60, 20 km for grid 1, 2, 3
EXP4 (adjusted weight)	terain adjusted nudging weights
EXP5 (nudging factor)	G_α=$2x10^{-3}$ s^{-1} on grid 3

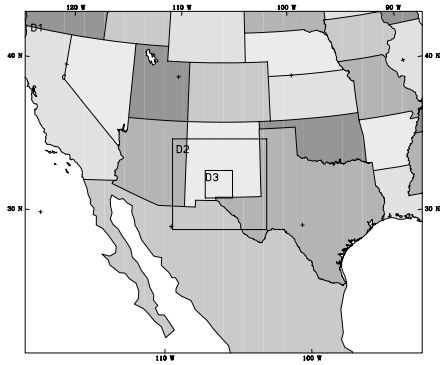

Figure 2 Domain configuration in RT-FDDA at WSMR.

Among the experimental runs, EXP2 is conducted to estimate the total impact of observational nudging on grid 3. In EXP3, the horizontal radius of influence R is reduced on grid 2 and 3 such that R for each grid is consistent with the grid resolution.

Terrain dependent weights (EXP4 in Table 1) are designed to eliminate the influence of an observation to a grid point if the two sites are physically separated by a mountain ridge or a deep valley. For a given observation and grid point, a terrain search is done along the line connecting the grid point and the observation site. If there is a terrain blockage or a valley (depth > 500 m), the nudging weight for the observation at the given grid point is set to zero. Since the terrain features affect surface observations most, we have tested the algorithm for nudging surface observations only.

The sensitivity experiments are evaluated through error statistics, local feature identification, and point observation comparison. To objectively assess the impact of the nudging parameters, verification statistics are calculated for the analysis/forecasts against a subset of the rawinsonde and surface observations that is withheld from the data assimilation. Fine scale features in grid 3, especially the surface fields (10 m wind U10, V10, 2 m temperature and moisture fields T2, Q2) are emphasized in the evaluation.

4. RESULTS OF THE EXPERIMENTS

The overall impact of grid 3 nudging and varying nudging parameters are first evaluated by calculating the domain average differences between the experimental runs and the control run. Fig. 3 shows such differences for grid 3 surface temperature and wind (vector, denoted as VT10 thereafter) fields. The differences between EXP2 and EXP1 reflect the total impact of grid 3 nudging, and the differences between EXP3-5 and EXP1 reflect the impact of changing the nudging parameters.

For both surface temperature and wind, the impact sizes exhibit daily cycles. The impact is the largest during early afternoon hours when the locally induced features are most prominent. Similar daily cycles are also seen in the Q2 field (not shown).

The maximum domain average effect caused by grid 3 observational nudging is about 2.8 K on T2 and 5 ms^{-1} on VT10 (solid lines). When the horizontal radius of influence is reduced (EXP3), the impact on T2 is about 1/2 of the total nudging impact. When terrain-adjusted weights are used (EXP4), the impact size is further reduced and is about 0.8 K for T2 and 3.2 ms^{-1} for VT10. When the nudging coefficient is changed (EXP5), a relatively large impact is also seen, especially in VT10.

The magnitudes of the various curves for VT10 are closer to each other than those for T2, reflecting a larger sensitivity of the wind to changes in the influence radius, nudging weights and nudging coefficient.

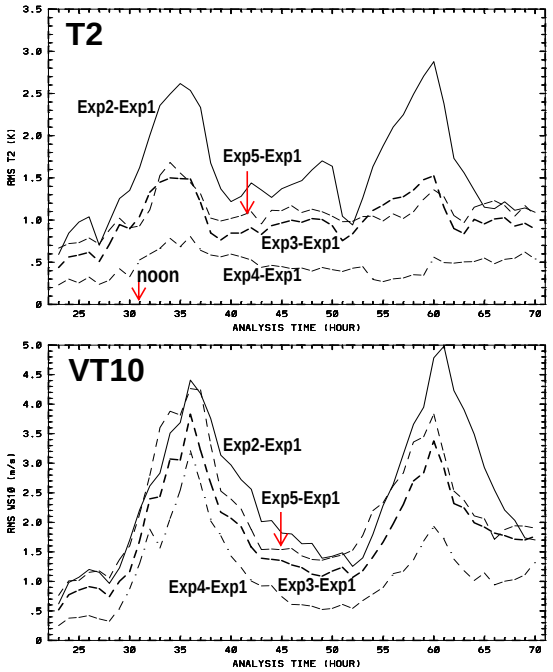

Figure 3 Root-mean-square differences between experimental and control runs for surface temperature T2 and wind VT10 respectively. Plotted are differences between: EXP1/EXP2 (solid), EXP3/EXP1 (heavy dashed), EXP4/EXP1 (dotted-dashed), and EXP5/EXP1 (thin dashed).

The local structures of the difference fields can be significantly stronger than the domain average values. Fig. 4 shows the instantaneous difference fields between EXP3,4 and EXP1 at 21 Z (33 h from cold start; 2 pm local time). In both EXP3 and EXP4, the maximum local wind changes (from the control) can be as large as 12 ms^{-1}, and the temperature differences can reach 4-5 C.

The structures are correlated to the terrain features (Fig. 4c). Although not all the features in the difference fields can be readily explained, some of them are corroborated by individual observations. For example, both EXP3 and EXP4 produce higher T2 in the upper right corner of the domain (eastern slopes of the mountains -area marked B in Fig. 4c). Surface observations in this region show that the control run has a large cold bias of about -6 C at the hour. With terrain-adjusted weights, the cold bias is reduced to about -4 C.

In general, MM5 is known to produce cold bias at noon and warm bias at midnight, which tends to reduce the amplitude of daily temperature variation. From this perspective, the colder temperatures in the central valley of grid 3 from EXP3 (Fig. 4a) is somewhat undesirable. We have examined the time series of T2 at selected grid points and averaged over domain 3 (not shown). Nudging on grid 3 clearly enhances the daily cycle of T2 (EXP1 vs EXP2). When terrain-adjusted weights are used, the amplitude of the cycle is preserved or slightly further enhanced. However, when R is simply reduced (EXP3), the amplitude of the cycle is slightly reduced.

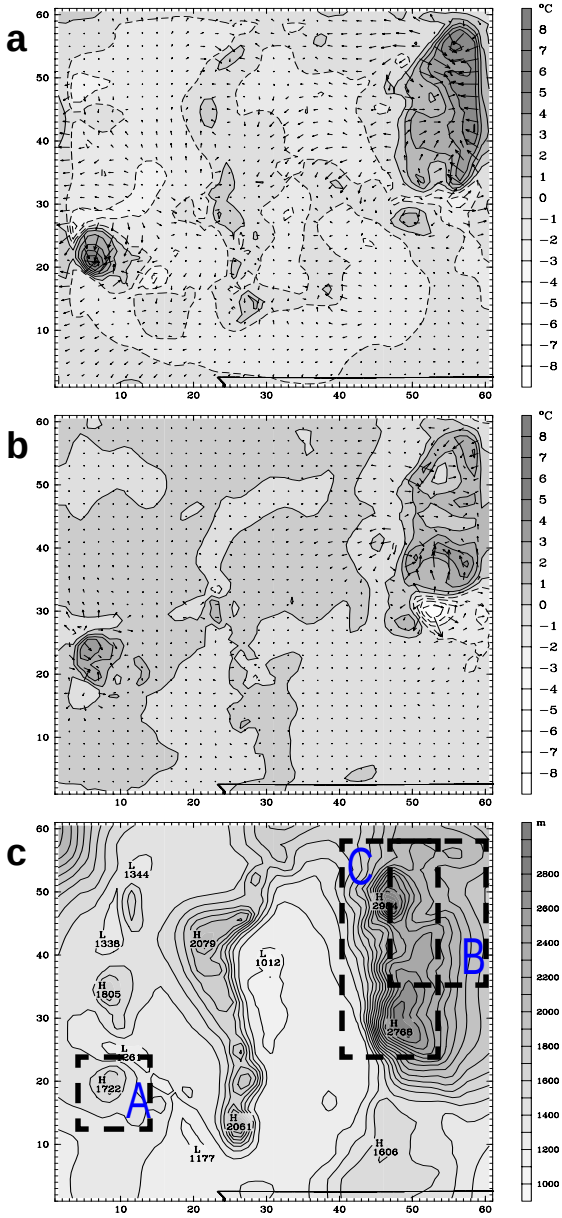

Figure 4 Differences of surface temperature (T2, contour) and wind (VT10, vector) between (a) EXP3 and EXP1, (b) EXP4 and EXP1 at 14 MST. The contour intervals are 1 C. The maximum vector is 12 ms^{-1}. (c) Grid 3 terrain.

The local circulation is another feature of interest. There are two regions of significant wind changes in Fig. 4. In region A (near a hill top), the convergence is significantly enhanced in EXP3 and EXP4. Region B is associated with a larger mountain range. Examination of the mean convergence at the mountain top (Fig. 5) shows that without nudging on grid 3, the local upslope circulation starts to develop around 10 am. When nudging is performed on grid 3, the local circulations become much stronger. The terrain-adjusted weights slightly affect the mean convergence around this mountain top while creating large local wind changes on the slopes (Fig. 4b).

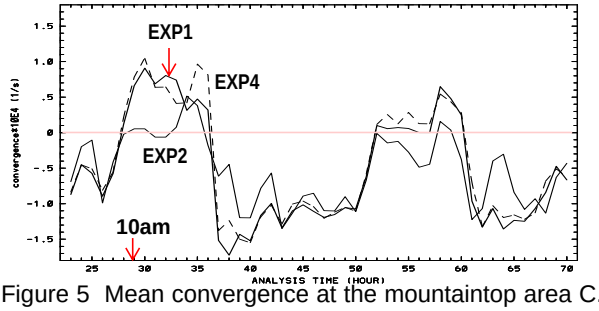

Figure 5 Mean convergence at the mountaintop area C. The curves are for EXP1, EXP2, and EXP4, respectively.

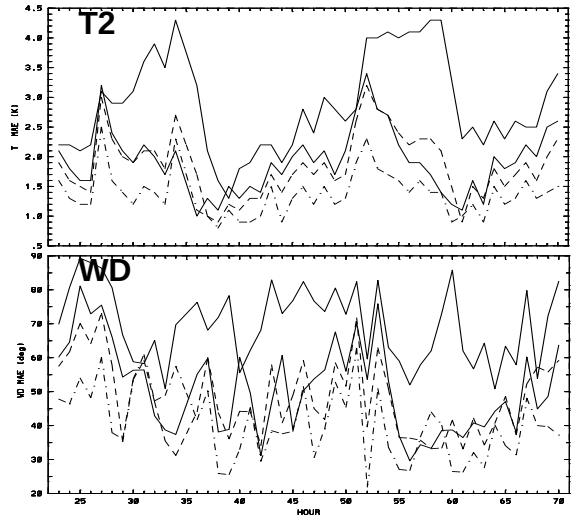

Figure 6 Hourly verification statistics on grid 3: mean absolute error in T2 and WD (wind direction) for EXP1 (heavy solid), EXP2 (thin solid), EXP3 (dashed) and EXP5 (dotted dashed).

Verification statistics are calculated against surface observations for the analysis cycles (Fig. 6 and Table 2). Approximately 15 observations in grid 3 are withheld from assimilation and used for verification at each hour. Given the local and discrete nature of the observations, the verification statistics may not be viewed as an absolute measure of the quality of the analysis fields.

A small improvement in statistics is seen when a reduced R is used. Among the variables affected by R, Q2 is the most improved (Table 2). This may be due to high spatial variability of Q2. A slightly reduced MAE is also seen when terrain-adjusted weights are used (Table 2).

When a larger nudging coefficient G_α is used, the verification errors are significantly reduced. This is natural because the model fields are forced more strongly toward the observations. Again this is not necessarily an indication that a larger G_α produces better model analysis. In fact a faster error growth in the forecast period is seen when a larger G_α is used. A more rigorous evaluation of the forecasts is needed in order to find the optimal nudging coefficient.

Table 2. Verification statistics for the analysis fields. Listed are the mean absolute errors in surface temperature (T2), wind speed (WS), wind direction (WD) and moisture (Q2) for grid 3 in the 48 h analysis period.

EXPNAME	e(T2)	e(WS)	e(WD)	e(Q2)
EXP1	1.88	1.06	49.95	0.43
EXP2	2.81	1.20	68.54	0.78
EXP3	1.81	1.03	47.06	0.35
EXP4	1.84	1.08	48.54	0.41
EXP5	1.34	0.97	39.82	0.23

5. SUMMARY AND FUTURE WORK

Sensitivity simulations are conducted for a clear-sky event by changing the nudging parameters in a mesoscale FDDA system. The results show that a significant change can be caused by varying the nudging parameters. Reduced radii of influence and terrain-adjusted nudging weights are shown to produce certain reasonable effects in the final analysis and slightly improved verification statistics.

Many questions remain to be answered, such as whether different nudging parameters should be used when nudging different observation types. Additional sensitivity tests and more case studies, need to be conducted. Eventually, parallel real-time runs using different nudging parameters need to be performed in order to fully assess the impact of the parameters on the analysis fields as well as forecast fields.

ACKNOWLEDGEMENT

This work was funded by the U. S. Army Test and Evaluation Command (ATEC).

REFERENCES

Cram, J. M., Y. Liu, S. Low-Cram, R.-S. Sheu, L. Carson, C. Davis, T. Warner, J. Bowers, 2001: An operational mesoscale RT-FDDA analysis and forecasting system. Preprints, 14th Conference on Numerical Weather Prediction, Ft. Lauderdale, FL, 30 July - 2 August, 2001.

Liu, Y., and coauthors, 2002: Performance and enhancements of the NCAR/ATEC RT-FDDA system. Preprints, 15th Conference on Numerical Weather Prediction, San Antonio, TX. 12-16 August, 2002.